Multipulse Adaptive Coherence for Detection in Wind Turbine Clutter

POORIA PAKROOH, Member, IEEE
LOUIS L. SCHARF, Life Fellow, IEEE
MARGARET CHENEY, Senior Member, IEEE
Colorado State University, Fort Collins, CO. USA

ANDREW HOMAN, Member, IEEE
MATTHEW FERRARA, Member, IEEE
Matrix Research, Inc., Beavercreek, HO, USA

Radar tracking of aircraft targets at low elevation angles can be complicated by clutter from wind turbines, which we define to be clutter. In this paper, we study detection in a staring pulse-Doppler radar. By exploiting the second-order correlation structure of this wind-turbine clutter we derive a target detector that uses a sequence of adaptive coherence scores. The detector uses a multipulse coherence statistic consisting of an incoherent geometric average of coherently computed adaptive coherence scores. The detector compares favorably to a multipulse coherence detector that uses no modeling or estimation of the clutter.

Manuscript received November 21, 2016; revised June 9, 2017; released for publication June 12, 2017. Date of publication July 17, 2017; date of current version December 5, 2017.

DOI. No. 10.1109/TAES.2017.2727825

Refereeing of this contribution was handled by S. Watts.

This work was supported by the Air Force Office of Scientific Research under Contract FA9550-14-C-0053.

Authors' addresses: P. Pakrooh and M. Cheney are with the Department of Mathematics, Colorado State University, Fort Collins, CO 80523USA, E-mail: (Pooria.Pakrooh@gmail.com; Cheney@math.colostate.edu); A. Homan and M. Ferrara are with Matrix Research, Inc., Beavercreek, OH 45432,USA, E-mail: (Andrew.Homan@matrixresearch.com; Matthew.Ferrara@matrixresearch.com); L. L. Scharf is with the Department of Mathematics and the Department of Statistics, Colorado State University, Fort Collins, CO 80523 USA, E-mail: (Louis.Scharf@colostate.edu). *(Corresponding author: Andrew Homan.)*

I. INTRODUCTION

Wind turbine clutter presents a significant challenge to detect targets in civilian radar systems for weather and air traffic control [1], and military systems for early warning and perimeter defense [2]. Much work has been focused on the *forward problem* of numerically solving Maxwell's equations to estimate the effects of wind turbine clutter (WTC) given that everything is known (blade lengths, tilt parameters, materials, etc) *a priori* about the wind turbine(s) (see, e.g., [1], [3]–[6]). This paper, however, is focused on solving the *inverse problem* of properly whitening the WTC from measured radar data and using this whitened data to detect targets at low elevation angles.

A wind turbine farm can present a stronger target than a single aircraft, by orders of magnitude. Traditional clutter filtering methods do not work for wind turbines because the clutter filters either 1) assume a zero or fixed Doppler velocity to estimate the clutter power or 2) notch filter the received signal to remove the velocity spectrum containing clutter. Wind turbines can present a broad-spectrum, nonstationary velocity signature that is difficult to separate from the return of interest (such as that from an aircraft).

Mitigating the clutter from wind turbines is difficult because of their large radar cross section, their significant Doppler spread, and their many large modes of vibration that arise from stochastic forcing by the wind [7]–[9]. Some progress in fielded systems has been made [10], [11], [12]. Jahangir [11], [12] has described a staring radar system for detection and Doppler resolution in wind turbine clutter. This system forms a multiplicity of beams from a two-dimensional (2-D) sensor array and uses a sequence of signal processing steps to form 2-D target tracks. Using a signal processing chain termed holographic radar, the author is able to maintain target track in wind turbine clutter.

Today's clutter-mitigation algorithms for radar (such as the Gaussian model adaptive processing algorithm [13]) are effectively Doppler high-pass filters that do not sufficiently eliminate the WTC returns from the received signal without degradation of the target signal. For example, in their WTC-mitigation feasibility study, Butler and Johnson [14] and others [2] considered Doppler filters, image-domain filtering techniques such as range-Doppler constant false alarm rate (CFAR) detectors and track inhibitors, and knowledge-based range gating. Based on the results of [14], Jackson and Butler [15] outlined various mitigation strategies, which, in addition to the aforementioned filtering approaches, included suggestions to apply beamforming on receive and waveform design. Palmer *et al.* [16] have also advocated beamforming techniques to mitigate WTC coming from known directions.

Hood *et al.* [17], [18] developed a fuzzy-logic WTC detector that used statistical moments of the backscattered Doppler spectrum as features. Later, [19] used the fuzzy-logic detector in [17], [18] to exclude certain resolution cells from the estimate of the target power spectral density. This processing chain is similar to knowledge-aided space-time adaptive processing [20]. Another WTC detector was

developed in [21], wherein log power ratios of pixels in range-Doppler images are used to identify the presence of WTC by classifying sharp changes in the Doppler spectrum (as measured by the log power ratio) as clutter.

In [22], Gallardo-Hernando *et al.* assume that the range-Doppler spectrum of the WTC is known *a priori*, notch out the wind-turbine returns and interpolate across the missing values in the filtered range-Doppler maps. Isom *et al.* [23], [24] use a similar notch-then-interpolate technique, except theirs extends the interpolation to three dimensions (range, azimuth, and Doppler) using multiquadric interpolation.

In [25], Naqvi and Ling present results for the (theoretically ideal) model-then-subtract approach to WTC mitigation. In particular, each blade is modeled as a summation of point scatterers in order to adequately simulate the polarimetric response of a wind turbine. The precise amplitudes of the point scatterers are determined on-the-fly using a greedy basis pursuit algorithm, and the model is used to detect a moving target in synthetic WTC data. Uysal *et al.* [26] also use a sparse signal model for the WTC, but their approach exploits a simpler short-time Fourier transform (STFT) basis, in which sparse STFT coefficients indicate the presence of WTC. Thus, although some progress in fielded systems has been made [10], in general the problem remains open.

In this paper, as in [25], [26] and others, we consider a staring radar with clutter from wind turbines in its field of view. We derive a detector that uses a sequence of adaptive coherence estimate (ACE) scores [27]–[30], and geometrically averages them to compute a multipulse coherence statistic. This statistic is called a multipulse ACE (MPACE), for its close connection to ACE. The detector is firmly grounded in detection theory in the multivariate normal model. Its innovation is its use of incoherent geometric averages of coherent ACE scores, based on target and clutter modeling. MPACE scores may be computed in the time domain or the frequency domain.

All of our analysis assumes additive, first-order scattering from wind turbine scattering centers. This assumption neglects any multiple scattering.

II. RADAR SIGNAL MODELS

We begin with the radio-frequency (RF) signal transmitted from a radar antenna

$$s(t) = \mathrm{Re}\left\{w(t)e^{j2\pi f_c t}\right\},\ \mathrm{supp}\, w(t) = [0, T_w]. \quad (1)$$

Here f_c is the carrier frequency in Hertz and w is the complex baseband signal. The impulse response h_k of the kth scatterer is modeled as a point scatterer, located at range R_k, and with (real-valued) gain a_k

$$h_k(t) = a_k \delta(t - \tau_k). \quad (2)$$

The time delay to scatterer k is $\tau_k = 2R_k/c$, where c is the speed of light. Here we use the start–stop approximation, also called the "stop-and-hop" approximation, which is the assumption that the scatterer is stationary during the time it interacts with each pulse, so that the motion takes place only between pulses, i.e., on the slow time scale. The convolution of the RF signal s with h_k produces the RF signal measured at the receiver

$$\begin{aligned} d_k(t) &= \int h_k(t - t')s(t')\, dt' = a_k s\,(t - \tau_k) \\ &= a_k \mathrm{Re}\left\{w\,(t - \tau_k)\, e^{j2\pi f_c(t-\tau_k)}\right\} \\ &= \mathrm{Re}\{\underbrace{\beta_k w(t - \tau_k)}_{z_k(t)}\, e^{j2\pi f_c t}\} \end{aligned} \quad (3)$$

where β_k is the complex gain

$$\beta_k = a_k e^{-j2\pi f_c \tau_k}. \quad (4)$$

We take it as a simple matter to extract the baseband signal $z_k(t)$ using a phase splitter, or using a complex demodulator, followed by a low-pass filter. So, after this front-end RF processing, all receiver processing is done at baseband, i.e., on a cluttered version of the signal $z_k(t) = \beta_k w(t - \tau_k)$.

The received baseband signal z_k may be aligned with the hypothesized delay τ, to obtain $z_k(t + \tau)$, and then correlated with the transmitted baseband signal $w(t)$

$$x_k(\tau) = \int \overline{w}(t) z_k(t + \tau)\, dt = \int \tilde{w}(t) z_k(\tau - t)\, dt. \quad (5)$$

This is the output of the time-reversed complex conjugate filter $\tilde{w}(t) = \overline{w}(-t)$ (where the bar denotes complex conjugation), excited by the demodulated signal $z_k(t)$ and read at time τ. Typically, this cross-correlation function is read at delays $\tau = \frac{\ell}{2W}$, $\ell = 0, 1, 2, \ldots$, where W is the bandwidth of the signal w.

By plugging into (5) the baseband formula for z_k from (3), we obtain the following formula for the cross-correlation x_k

$$x_k(\tau) = \beta_k \int \overline{w}(t) w(t + \tau - \tau_k)\, dt\ = \beta_k A_{ww}(\tau - \tau_k) \quad (6)$$

where $A_{ww}(\tau)$ is the auto-correlation function of w

$$A_{ww}(\tau) = \int \overline{w}(t) w(t + \tau)\, dt = \int \tilde{w}(t) w(\tau - t) dt. \quad (7)$$

The rightmost integral shows that cross-correlation is the output of a pulse compression filter, sampled at τ. With K scatterers, the formula for $x(\tau)$ is

$$x(\tau) = \sum_{k=1}^{K} \beta_k A_{ww}(\tau - \tau_k). \quad (8)$$

If a sequence of pulses is transmitted, and the carrier phase is maintained throughout the sequence, then this formula holds for all pulses, except for the fact that the delay associated with the kth scatterer has changed to $\tau_k[p]$, where p is the index of the pth pulse. The linear combination of scattered returns from pulse p is then

$$x(\tau; p) = \sum_{k=1}^{K} \beta_k[p] A_{ww}(\tau - \tau_k[p]) \quad (9)$$

where

$$\beta_k[p] = a_k[p]e^{-j2\pi f_c \tau_k[p]} = a_k[p]e^{j\theta_k[p]} \tag{10}$$

$$\theta_k[p] = -2\pi f_c \tau_k[p]. \tag{11}$$

If the kth scatterer is moving with constant down-range velocity v_k, then $\tau_k[p] = \tau_k[0] + 2pTv_k/c$, assuming time T elapses between pulses.

III. TARGET AND CLUTTER MODEL

The complex scattering coefficient $\beta_k[p]$, delay $\tau_k[p]$, and velocity v_k are our objects of interest. From here on, it is the modeling of these quantities that distinguishes target from clutter. Our approach will be to model the second-order statistics of x for clutter, and the first-order statistics of x for target, so that an ACE statistic [27]–[30] may be computed as the score assigned to each cell of the range-Doppler plane. We use the following models for the phase $\theta_k[p]$.

A. Wind Turbine

We begin with the receiver output (9) for pulse p, now denoted $c(\tau; p)$ to emphasize that we are modeling wind turbine clutter

$$c(\tau; p) = \sum_{k=1}^{K} a_k[p]e^{j\theta_k[p]} A_{ww}\left(\tau - \tau_k[p]\right). \tag{12}$$

We assume that the scattering coefficients $a_k[p]e^{j\theta_k[p]}$ and $a_\ell[q]e^{j\theta_\ell[q]}$ are uncorrelated over scatterers, for all pulse numbers (p, q). That is

$$\mathbb{E}\left[a_k[p]e^{j\theta_k[p]}\overline{a}_\ell[q]e^{-j\theta_\ell[q]}\right] = A[p, q; k]\delta[k, \ell] \tag{13}$$

where

$$A[p, q; k] = \mathbb{E}\left[a_k[p]\overline{a}_k[q]e^{j(\theta_k[p]-\theta_k[q])}\right] \tag{14}$$

is the correlation between the scattering coefficient of scatterer k as it moves and is scanned by pulses p and q. The corresponding formula for the correlation $C[p, q]$ between receiver outputs is

$$C[p, q] = \mathbb{E}[c(\tau; p)\overline{c}(\tau; q)] \tag{15}$$

$$= \sum_{k=1}^{K} A[p, q; k]A_{ww}(\tau - \tau_k[p])\overline{A}_{ww}(\tau - \tau_k[q]). \tag{16}$$

Now, as we track the kth scatterer, we note that it returns to its approximate original position, arbitrarily defined, every M pulse trains of length R (i.e., MR pulses), and therefore, the statistics of the radar returns from the kth scatterer repeat every MR pulses. Then the correlation function A is periodic in (p, q), which is to say that for all k

$$A[p + MR, q + MR; k] = A[p, q; k] \tag{17}$$

and therefore

$$C[p + MR, q + MR] = C[p, q]. \tag{18}$$

We conclude that radar returns from the wind turbine are periodically correlated, with long period MR. This means that the clutter model for MR pulses may be used repeatedly for consecutive pulse trains consisting of MR pulses. By way of example, for the system described in Section V, $T = 1$ msec, and the wind turbine, which has three blades, undergoes a full rotation about every 2 s. Consequently, the number of pulses in $1/3$ of a turbine rotation is about $2000/3$. Thus, for $R = 20$ and $MRT = 2/3$ s, the resulting value of M is $M = 100/3 \approx 33$. So by organizing radar returns into blocks of $33 \cdot 20 = 660$ pulses, we may treat each such consecutive block as if its clutter component had the same correlation structure as every other such block.

This reasoning holds for clutter from a single turbine. For a wind turbine farm of turbines that are unsynchronized in rate and phase, we expect the clutter to be wide sense stationary over many periods of any one of the turbines (A periodically correlated time series, randomly time delayed over its period is WSS). This means the clutter covariance can still be estimated from secondary data and each $MR \times MR$ covariance matrix may still be approximated to be block diagonal with block sizes $KR \times KR$. The parameter MR no longer has the interpretation of number of pulses in $1/3$ turbine period, but this is immaterial. It just determines the number of ACE scores to be geometrically averaged. In many cases it seems reasonable to expect that weather conditions near the turbine will remain relatively stable over periods on the order of tens of seconds, which is enough to estimate periodically correlated clutter or wide-sense stationary clutter.

B. Constant Velocity Target

We consider a target with constant down-range velocity v on the time interval $[0, MRT]$. These MR pulses correspond to M consecutive pulse trains, each train a sequence of R pulses. Within each of these trains, the phase of the target return advances linearly, but after R such pulses, we assume that phase coherence is lost. At this point a new train begins. The resulting set of MR pulses accounts for the number of pulses transmitted and received in $1/3$ of a turbine period. We parameterize the index for the pth transmitted pulse on the time interval $[0, MRT]$ as $p = mR + r$, $m = 0, 1, \ldots, M-1$; $r = 0, 1, \ldots, R-1$. That is, p denotes the rth pulse in the mth pulse train. The time delay for this pulse is then

$$\tau[r, m] = \tau[0, 0] + (mR + r)2vT/c. \tag{19}$$

The corresponding phase delay for the rth pulse in the mth pulse train is

$$\begin{aligned}\phi[r, m] = &-2\pi f_c \tau[r, m] = -2\pi f_c\big(\tau[0, 0] \\ &+ (mR + r)2vT/c\big) \\ = &\,\phi[0, m] + r\theta\end{aligned} \tag{20}$$

where $\phi[0, m] = -2\pi f_c \tau[0, 0] + mR\theta$, and $\theta = -2\pi f_c(2Tv/c)$. Now, assuming the real scattering coefficient of the target during the transmission of pulses in the mth pulse train is constant at $a[m]$, the complex scattering

coefficient for the rth pulse in the mth pulse train is

$$\begin{aligned}\beta[r,m] &= a[m]e^{j\phi[r,m]} \\ &= a[m]e^{j\phi[0,m]}e^{jr\theta} \\ &= \beta[m]e^{jr\theta}\end{aligned} \tag{21}$$

where $\beta[m] = a[m]e^{j\phi[0,m]}$. Thus, for the pulse $p = mR + r$, from (20) and (21), the formula for x is

$$x(\tau; mR + r) = \beta[m]e^{jr\theta}A_{ww}(\tau - \tau[r,m]). \tag{22}$$

When discrete-Fourier transformed, the result is

$$\begin{aligned}\hat{x}(\tau; m, e^{j\Omega}) &= \sum_{r=0}^{R-1} x(\tau; mR + r)e^{-j\Omega r} \\ &= \beta[m]A_{ww}(\tau - \tau[0,m])e^{-j(\Omega-\theta)(R-1)/2} \\ &\quad \times \frac{\sin[(\Omega-\theta)R/2]}{\sin[(\Omega-\theta)/2]}\end{aligned} \tag{23}$$

assuming $A_{ww}(\tau - \tau[r,m])$ is constant at $A_{ww}(\tau - \tau[0,m])$ for $r = 0, 1, \ldots, R-1$. We have used the argument $e^{j\Omega}$ on the left side of (23) to remind us that $\hat{x}$ is periodic in Ω, with period 2π. Formula (23) shows that $\theta \leq 2\pi$ is resolved at resolution $\frac{2\pi}{R}$. So resolution increases linearly with the number of pulses R over which these assumptions hold. For unaliased resolution of v (which is our objective), the phase advance per pulse must be less than or equal to 2π, which is to say, for $\lambda_c = \frac{c}{f_c}$

$$0 < 2\pi\frac{2vT}{\lambda_c} \leq 2\pi \quad \text{or} \quad 0 < vT \leq \frac{\lambda_c}{2}. \tag{24}$$

That is, the target must not travel more than a half-wavelength $\lambda_c/2$ of the carrier wave between pulse transmissions. This places a constraint on the radar design: for example, a carrier frequency corresponding to a wavelength of $\lambda_c = 10$ cm and a pulse repetition rate of 1 KHz has a maximum unambiguous velocity of 50 m/s, or a maximum unambiguous velocity range of ± 25 m/s.

IV. TARGET DETECTION

Once pulses have been organized as described in Section III, the problem is to develop a complex, proper, multivariate normal model for the data, where the target signature enters the mean and the clutter correlation enters the covariance. Based on this model, we derive a generalized likelihood ratio (GLR) test that can be constructed from any available training data that is used to identify the unknown clutter correlation. In this derivation we do not enforce phase continuity between consecutive pulse trains. We do, however, assume that target velocity and, therefore, linear phase increase are constant over $3MR$ pulses, which is the number of pulses transmitted in one rotation of a typical three-bladed wind turbine.

As discussed in Section III, we assume that the target return is an incoherent sequence of M coherent pulse trains, each train consisting of R phase-coherent pulses. Based on (22), we denote the target return for the mth train as

$$\psi_R(\theta)\beta[m], \quad m = 0, 1, \ldots, M-1 \tag{25}$$

where $\psi_R(\theta) = [1, e^{j\theta}, \ldots, e^{j(R-1)\theta}]^T \in \mathbb{C}^R$ and $\beta[m] = a[m]e^{j\phi[0,m]}$. We assume $A_{ww}(\tau - \tau[r,m])$ is approximately constant at the value $A_{ww}(\tau - \tau[0,m])$, for each m, as the target is assumed to remain in a fixed range-Doppler cell over the time duration of any pulse train. Thus, we may absorb this constant into $\beta[m]$. We organize the returns of coherent pulse trains plus wind turbine clutter as $\mathbf{y} = [\mathbf{y}_0^T, \mathbf{y}_1^T, \ldots, \mathbf{y}_{M-1}^T]^T \in \mathbb{C}^{MR}$, with each $\mathbf{y}_m \in \mathbb{C}^R$, and form a hypothesis test on $\mathbf{y}$ for the detection of the target in the presence of wind turbine clutter. We hypothesize the distribution of $\mathbf{y}$ under each hypothesis as

$$\begin{aligned}H_0 &: \mathbf{y} \sim \mathcal{CN}_{MR}(\mathbf{0}, \mathbf{R}) \\ H_1 &: \mathbf{y} \sim \mathcal{CN}_{MR}(\boldsymbol{\beta} \otimes \psi_R(\theta), \mathbf{R})\end{aligned} \tag{26}$$

where $\boldsymbol{\beta} = [\beta[0], \beta[1], \ldots, \beta[M-1]]^T \in \mathbb{C}^M$ and $\otimes$ denotes Kronecker product. Here, $\mathbf{R} \in \mathbb{C}^{MR\times MR}$ is the covariance matrix of the zero-mean scattered signal from wind turbines. In order to fix notation, we give $\mathbf{R}$ the following pattern:

$$\mathbf{R} = \begin{bmatrix} \mathbf{R}_{00} & \mathbf{R}_{01} & \cdots & \mathbf{R}_{0(M-1)} \\ \mathbf{R}_{01}^H & \mathbf{R}_{11} & \cdots & \mathbf{R}_{1(M-1)} \\ \vdots & & \ddots & \vdots \\ \mathbf{R}_{0(M-1)}^H & \cdots & \cdots & \mathbf{R}_{(M-1)(M-1)} \end{bmatrix}. \tag{27}$$

The covariance block $\mathbf{R}_{mn} \in \mathbb{C}^{R\times R}$ is $\mathbf{R}_{mn} = \mathbb{E}[\mathbf{y}_m\mathbf{y}_n^H]$ under H_0, for $m, n \in \{0, 1, \ldots M-1\}$. In the subsections to follow, we derive two different detectors, each corresponding to a particular approximation to $\mathbf{R}$ in (27).

A. Coherence Detector Using MPACE Scores

As an approximation, we might say $\mathbf{R}$ is block diagonal with N blocks of size KR, and $NKR = MR$. So, there are N blocks on the diagonal, each of size $KR \times KR$. Then, we have the approximation

$$\mathbf{R} = \text{blkdiag}\left[\mathbf{Q}_{00}, \mathbf{Q}_{11}, \ldots, \mathbf{Q}_{(N-1)(N-1)}\right] \tag{28}$$

where $\mathbf{Q}_{nn} = \mathbb{E}[\mathbf{w}_n\mathbf{w}_n^H] \in \mathbb{C}^{KR\times KR}$ under H_0, and $\mathbf{w}_n^T = [\mathbf{y}_{nK}^T, \ldots, \mathbf{y}_{(n+1)K-1}^T]^T$. This model amounts to an approximation that clutter is uncorrelated for pulse trains separated by more than K trains. With this approximation, $\mathbf{w}_n$'s are independent for $n \in \{0, \ldots N-1\}$, each distributed as

$$\begin{aligned}H_0 &: \mathbf{w}_n \sim \mathcal{CN}_{KR}(\mathbf{0}, \mathbf{Q}_{nn}) \\ H_1 &: \mathbf{w}_n \sim \mathcal{CN}_{KR}(\boldsymbol{\beta}_n \otimes \psi_R(\theta), \mathbf{Q}_{nn})\end{aligned} \tag{29}$$

and $\boldsymbol{\beta}_n = [\beta[nK], \ldots, \beta[(n+1)K-1]]^T \in \mathbb{C}^K$. The mean may be written as

$$\boldsymbol{\beta}_n \otimes \psi_R(\theta) = \Psi_{KR}(\theta)\boldsymbol{\beta}_n \tag{30}$$

where $\Psi_{KR}(\theta) = \mathbf{I}_K \otimes \psi_R(\theta) \in \mathbb{C}^{KR\times K}$. Thus, the hypothesis test for the random vectors $\mathbf{w}_0, \ldots, \mathbf{w}_{N-1}$ may be written as

$$\begin{aligned}H_0 &: \mathbf{w}_n \sim \mathcal{CN}_{KR}(\mathbf{0}, \mathbf{Q}_{nn}) \\ H_1 &: \mathbf{w}_n \sim \mathcal{CN}_{KR}(\Psi_{KR}(\theta)\boldsymbol{\beta}_n, \mathbf{Q}_{nn})\end{aligned} \tag{31}$$

where $n = 0, 1, \ldots, N-1$ and $N = M/K$. This is the basic hypothesis-testing model for which we derive a GLR test.

Now, we give ourselves a training sample of L copies of $\mathbf{z}_l \sim \mathcal{CN}_{MR}(\mathbf{0}, \mathbf{R}_{zz})$ under H_0, for $L \geq KR$, where

$$\mathbf{R}_{zz} = \text{blkdiag}\left[\sigma_0^2\mathbf{Q}_{00}, \sigma_1^2\mathbf{Q}_{11}, \ldots, \sigma_{(N-1)}^2\mathbf{Q}_{(N-1)(N-1)}\right] \tag{32}$$

for some unknown set of relative scalings $\{\sigma_0^2, \sigma_1^2, \ldots, \sigma_{N-1}^2\}$. Partitioning the training data matrix as $\mathbf{Z} = [\mathbf{z}_0, \ldots, \mathbf{z}_{L-1}] = [\mathbf{Z}_0^T, \ldots, \mathbf{Z}_{N-1}^T]^T, \mathbf{Z}_n \in \mathbb{C}^{KR\times L}$, the GLR for the hypothesis test in (31) is

$$\begin{aligned}\Lambda &= \frac{\max_{\{\sigma_n^2, \beta_n, \mathbf{Q}nn\}_{n=0}^{N-1}} f_{H_1}(\mathbf{W}, \mathbf{Z})}{\max_{\{\sigma_n^2, \mathbf{Q}nn\}_{n=0}^{N-1}} f_{H_0}(\mathbf{W}, \mathbf{Z})} \\ &= \prod_{n=0}^{N-1} \frac{\max_{\sigma_n^2, \beta_n, \mathbf{Q}nn} f_{H_1}(\mathbf{w}_n, \mathbf{Z}_n)}{\max_{\sigma_n^2, \mathbf{Q}nn} f_{H_0}(\mathbf{w}_n, \mathbf{Z}_n)}\end{aligned} \tag{33}$$

where the probability density functions (pdfs) $f_{H_0}(\mathbf{W}, \mathbf{Z})$ and $f_{H_1}(\mathbf{W}, \mathbf{Z})$ are the joint pdfs of the test data $\mathbf{W} = [\mathbf{w}_0, \ldots, \mathbf{w}_{N-1}]$ under H_0 and H_1, respectively, and the training data $\mathbf{Z} = [\mathbf{Z}_0^T, \ldots, \mathbf{Z}_{N-1}^T]^T$. In a similar manner as in [29], by replacing the unknown parameters $\{\sigma_n^2, \boldsymbol{\beta}_n, \mathbf{Q}_{nn}\}_{n=0}^{N-1}$ with their ML estimates under each hypothesis in (33), we have

$$\frac{1}{\Lambda^{1/R}} = \prod_{n=0}^{N-1}(1 - \rho_n^2) \tag{34}$$

or equivalently

$$1 - \frac{1}{\Lambda^{1/R}} = 1 - \prod_{n=0}^{N-1}(1 - \rho_n^2) \tag{35}$$

where $\rho_n^2 = \frac{\mathbf{v}_n^H \mathbf{P}_{\mathbf{G}_n} \mathbf{v}_n}{\mathbf{v}_n^H \mathbf{v}_n}$, $\mathbf{v}_n = \tilde{\mathbf{Q}}_{nn}^{-1/2}\mathbf{w}_n$, $\tilde{\mathbf{Q}}_{nn} = \frac{1}{L}\mathbf{Z}_n\mathbf{Z}_n^H$ is the sample covariance matrix for the nth block, and $\mathbf{G}_n = \tilde{\mathbf{Q}}_{nn}^{-1/2}\Psi_{KR}(\theta)$.

We call the detector statistic of (35) *multipulse adaptive coherence*, or MPACE. It is one minus a product of sine-squared terms, and each sine-squared term is one minus an ACE score, which is itself a coherence score. Note that we are free to choose K in our experiments. Therefore, our detector consists of the product of $N = M/K$ time-domain ACE scores, ρ_n^2, each of which processes K pulse trains of duration R to form a cosine-squared statistic [27]–[30]. These scores have the virtue that they are invariant to scalings of the target signature ψ, and the time-domain variables $\mathbf{v}_n$. The detector in (34) is derived based on the approximation of $\mathbf{R}$ with a block-diagonal matrix with blocks of size KR, for some $1 \leq K \leq M$.

B. Coherence Detector Using Frequency Domain MPACE Scores

When the wind turbine covariance has block circulant structure, then a vector-valued Fourier transform will block diagonalize the covariance matrix. More generally, a vector-valued Fourier transform tends to promote diagonalization. In the idealized case that the Hermitian clutter covariance $\mathbf{R} \in \mathbb{C}^{MR\times MR}$ is block circulant, with blocks of size KR, $\mathbf{R}$ has the form

$$\mathbf{R} = \begin{pmatrix} \mathbf{R}[0] & \mathbf{R}[1] & \cdots & \mathbf{R}[N-1] \\ \mathbf{R}^H[1] & \mathbf{R}[0] & \cdots & \mathbf{R}[N-2] \\ \vdots & \vdots & \vdots & \vdots \\ \mathbf{R}^H[N-2] & \cdots & \cdots & \mathbf{R}[1] \\ \mathbf{R}^H[N-1] & \cdots & \cdots & \mathbf{R}[0] \end{pmatrix} \tag{36}$$

where $\mathbf{R}[n] \in \mathbb{C}^{KR\times KR}$ for $n = 0, \ldots, N-1$, and $\mathbf{R}[n] = \mathbf{R}^H[N-n]$. This block-circulant matrix has the discrete Fourier transform representation

$$\mathbf{R} = (\mathbf{V}_N \otimes \mathbf{I}_{KR})\mathbf{S}(\mathbf{V}_N \otimes \mathbf{I}_{KR})^H \tag{37}$$

where $\mathbf{V}_N$ is the (unitary) discrete Fourier transform matrix of dimension N, namely $(\mathbf{V}_N)_{k,l} = \frac{1}{\sqrt{N}}e^{j2\pi kl/N}$. The matrix $\mathbf{S} = \text{diag}[\mathbf{S}_0, \ldots, \mathbf{S}_{N-1}] \in \mathbb{R}^{MR\times MR}$ is a block diagonal matrix with blocks $\mathbf{S}_n \in \mathbb{C}^{KR\times KR}$, $n = 0, \ldots, N-1$, each consisting of a matrix-valued Fourier coefficient for the block-structured correlation sequence $\{\mathbf{R}[n] : n = 0, \ldots N-1\}$ in the first row of $\mathbf{R}$

$$\mathbf{S}_n = \sum_{l=0}^{N-1} \mathbf{R}[l]e^{-j\frac{2\pi ln}{N}} \in \mathbb{C}^{KR\times KR}, \quad n = 0, 1, \ldots, N-1. \tag{38}$$

Now, we define the transform $\hat{\mathbf{w}} = (\mathbf{V}_N \otimes \mathbf{I}_{KR})^H\mathbf{y}$. Here, $\hat{\mathbf{w}} = [\hat{\mathbf{w}}_0^T, \hat{\mathbf{w}}_1^T, \ldots, \hat{\mathbf{w}}_{N-1}^T]^T$ where each $\hat{\mathbf{w}}_k$ is given as

$$\hat{\mathbf{w}}_k = \sum_{n=0}^{N-1} \mathbf{w}_n e^{-j\frac{2\pi n}{N}k}, \quad k = 0, 1, \ldots, N-1 \tag{39}$$

and $\mathbf{w}_n^T = [\mathbf{y}_{nK}^T, \ldots, \mathbf{y}_{(n+1)K-1}^T]^T$. Therefore, each $\hat{\mathbf{w}}_k$, which is a vector-valued Fourier coefficient, is a coherent combination of the sequence $\{\mathbf{w}_n\}_{n=0}^{N-1}$, with corresponding $e^{-j\frac{2\pi n}{N}k}$ phasings. This Fourier transform has a fundamental frequency of $2\pi/N$, determined by the period of the block-circulant covariance matrix for the wind turbine clutter.

The random vectors $\hat{\mathbf{w}}_0, \ldots, \hat{\mathbf{w}}_{N-1}$ are independent, and distributed as

$$\begin{aligned} H_0 &: \hat{\mathbf{w}}_n \sim \mathcal{CN}_{KR}(\mathbf{0}, \mathbf{S}_n), \\ H_1 &: \hat{\mathbf{w}}_n \sim \mathcal{CN}_{KR}(\Psi_{KR}(\theta)\mathbf{b}_n, \mathbf{S}_n) \end{aligned} \tag{40}$$

with $n = 0, 1, \ldots, N-1$, where $\mathbf{b}_n = \sum_{m=0}^{N-1} \boldsymbol{\beta}_m e^{-j\frac{2\pi m}{N}n}$, and $\boldsymbol{\beta}_m = [\beta[mK], \ldots, \beta[(m+1)K-1]]^T$. Again, we give ourselves a training sample of L copies of $\mathbf{z}_l \sim \mathcal{CN}_R(\mathbf{0}, \mathbf{R}_{zz})$ under H_0, where $\mathbf{R}_{zz} = (\mathbf{V}_N \otimes \mathbf{I}_{KR})\mathbf{T}(\mathbf{V}_N \otimes \mathbf{I}_{KR})^H$, $\mathbf{T} = \text{blkdiag}[\gamma_0^2\mathbf{S}_0, \ldots, \gamma_{N-1}^2\mathbf{S}_{N-1}]$, and the scaling factors $\gamma_0^2, \ldots, \gamma_{N-1}^2$ are unknown. We define the training data matrix as $\mathbf{Z} = [\mathbf{z}_1, \ldots, \mathbf{z}_{L-1}]$, and partition the vector-valued Fourier transform of the data matrix as $\hat{\mathbf{Z}} = (\mathbf{V}_N \otimes \mathbf{I}_{KR})^H\mathbf{Z} = [\hat{\mathbf{Z}}_0, \ldots, \hat{\mathbf{Z}}_{N-1}^T]^T, \hat{\mathbf{Z}}_n \in \mathbb{C}^{KR\times L}$. Similar to (35), the GLR may be written as

$$\frac{1}{\Lambda^{1/R}} = \prod_{n=0}^{N-1}(1 - \hat{\rho}_n^2) \tag{41}$$

or equivalently

$$1 - \frac{1}{\Lambda^{1/R}} = 1 - \prod_{n=0}^{N-1} \left(1 - \hat{\rho}_n^2\right) \tag{42}$$

where $\hat{\rho}_n^2 = \frac{\hat{\mathbf{v}}_n^H \mathbf{P}_{\hat{\mathbf{G}}_n} \hat{\mathbf{v}}_n}{\hat{\mathbf{v}}_n^H \hat{\mathbf{v}}_n}$, $\hat{\mathbf{v}}_n = \tilde{\mathbf{S}}_n^{-1/2} \hat{\mathbf{w}}_n$, $\hat{\mathbf{G}}_n = \tilde{\mathbf{S}}_n^{-1/2} \Psi_{KR}(\theta)$, $\tilde{\mathbf{S}}_n = \frac{1}{L} \hat{\mathbf{Z}}_n \hat{\mathbf{Z}}_n^H$, and $\hat{\mathbf{w}}_n$ is given in (39). Throughout this derivation, the hat notation $\hat{\mathbf{w}}_n$ indicates a vector-valued Fourier transform of time-domain measurements. Therefore, our detector consists of the product of N frequency-domain ACE scores. These scores have the virtue that they are invariant to scaling of the target signature ψ, and the frequency-domain variables $\hat{\mathbf{w}}_n$.

These detectors account for MR pulses in 1/3 a turbine period. For subsequent periods, the time-domain estimated covariance matrices $\tilde{\mathbf{Q}}_{nn}$ or frequency-domain estimated covariance matrices $\tilde{\mathbf{S}}_n$, $n = 0, 1, \cdots, N-1$, may be reused for $n = 0 + \ell N, \ldots, N - 1 + \ell N$, for $\ell = 1, 2, \ldots, P$, until the changing aspect of the wind turbine forces a new training period to determine a new set of estimated covariance matrices.

V. RESULTS

A. CSU-CHILL

In order to test the target detectors designed in Section IV, we obtained a set of *S*-band, dual-polarization data from the CSU-CHILL National Weather Radar Facility located in Greeley, CO, USA and operated by Colorado State University. The system operates at a center frequency of 2.725 GHz, which corresponds to a wavelength of 11 cm. The transmitted waveforms are continuous wave pulses. The pulse repetition time is 1.042 msec ≈1 msec (pulse repetition frequency (PRF) of 960 Hz), and the system has 1-MHz bandwidth, which corresponds to a pulse duration of 1 μs = 10^{-6} s. We used $N = 99349 \approx 10^5$ pulses. This means the total data record has duration $\approx 10^5$ pulses $\times 10^{-3}$ s/pulse = 100 s. The CHILL radar system recorded returns with a maximum range of 75 km, aggregated into 500 range gates, each 150 m wide.

The radar was pointed toward the Ponnequin Wind Farm, about 63 km away. Although the wind farm contains both NEG and Vestas turbines, we focused our attention on range bin 435, which we believe contains only a single Vestas turbine. The Vestas turbines (model 47) rotate at only a single nonzero rate, namely 29 r/min. The blades are 77 ft long, and the pivot is 227 ft above the ground. These operate at a constant blade pitch, but the pitch changes to 90° when the blades stop rotating when the wind speed is too low or too high.

Fig. 1 shows the layout of the Ponnequin wind farm, with iso-range curves superimposed. The figure also shows the 150-m range bins and .1° beam demarcations. The beam width for the *S*-band radar data that we are using is 1°, so ten boxes correspond to the width of the beam. There are four lines of wind turbines totaling 44.

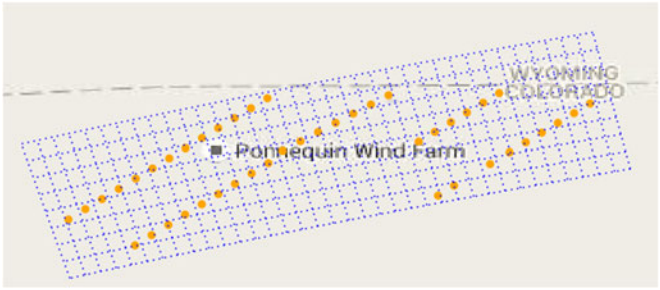

Fig. 1. Nominal map of the Ponnequin Wind Farm, near the Colorado-Wyoming border, with orange markers showing the turbine locations. The dotted blue lines are iso-range curves, with .1° beam demarcations. The beam width for the *S*-band radar data that we are using is 1°. Map data from Google.

B. Synthetic Linearly Translating Point Scatterer Superimposed Over Turbine Clutter

In the design of the MPACE detectors described in Section IV, there are three design parameters: R, M, and K. The choice of each parameter must be selected by the designer based on experimental evidence. The parameter R determines the number of pulses that may be coherently processed, and is determined by the scattering properties of the target. To assume a value of R is to assume that over time intervals of length RT, 1) the scattering coefficient of the target is roughly constant, and 2) the radar signal due to scattering from the target has a phase that changes approximately linearly with time. The larger R, the larger the coherent processing gain of each ACE score, and the finer the Doppler resolution, λ_c / RT. The choice of M assumes that the scattering field has a fixed correlation matrix over a time interval of length MRT, and the target remains within a fixed range cell over that interval, where the width of a range cell is determined by the transmitted pulse bandwidth. The larger M, the larger is the incoherent processing gain of consecutive ACE scores. The value of K determines an approximation of the clutter covariance as a block diagonal matrix, with blocks of size $KR \times KR$, for the purpose of whitening the clutter in the computation of MPACE scores.

As a practical matter, the application of the ACE detector requires a choice of parameters (R, M, K) based on experiments, and perhaps the computation of coherence scores for multiple values of (R, M, K). Thus, the coherence detector provides the designer control over these three parameters, whereas the unwhitened MPACE ($K = 1, \mathbf{R} = \mathbf{I}$), which we term MPCE for multipulse coherence estimator, provides only control over the parameters (R, M). Moreover, the MPACE detector uses secondary data to distribute clutter power evenly over the entire Doppler plane by whitening. The MPCE leaves the wind turbine clutter power distributed unevenly within its Doppler extent.

In Fig. 2, we record the STFT of the pulse history of the 435th range bin. It exhibits the characteristic periodicity associated with clutter from a wind turbine. After approximately 65 s, the orientation of the wind turbine changed, increasing the Doppler extent of the clutter. Empirically, the turbine period is 2.091 s (≈2007 pulses), which is

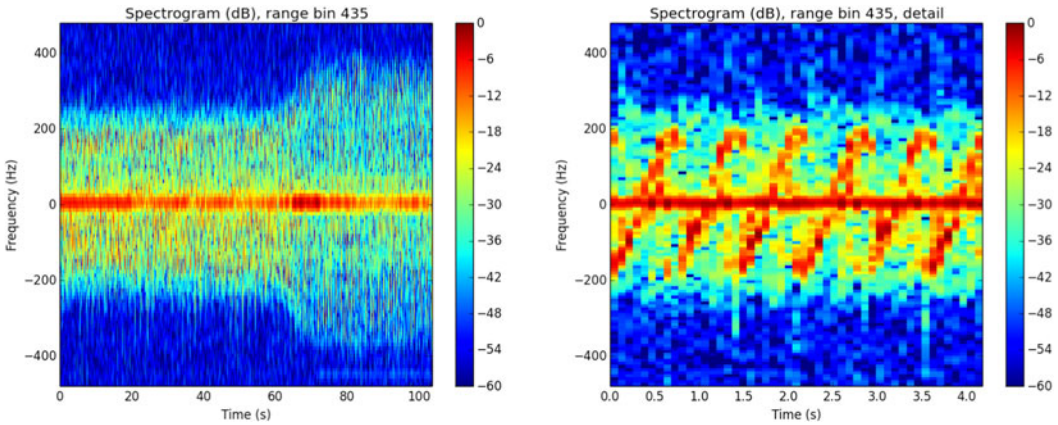

Fig. 2. (Left) STFT of the signal from range bin 435. (Right) Detailed short-time Fourier transform (STFT) of signal from range bin 435 over two full periods of turbine rotation, or approximately 4.18 s. The STFT was generated with a sliding Kaiser window ($\alpha = 1.5$) supported on forty pulses, with an overlap of 20 pulses.

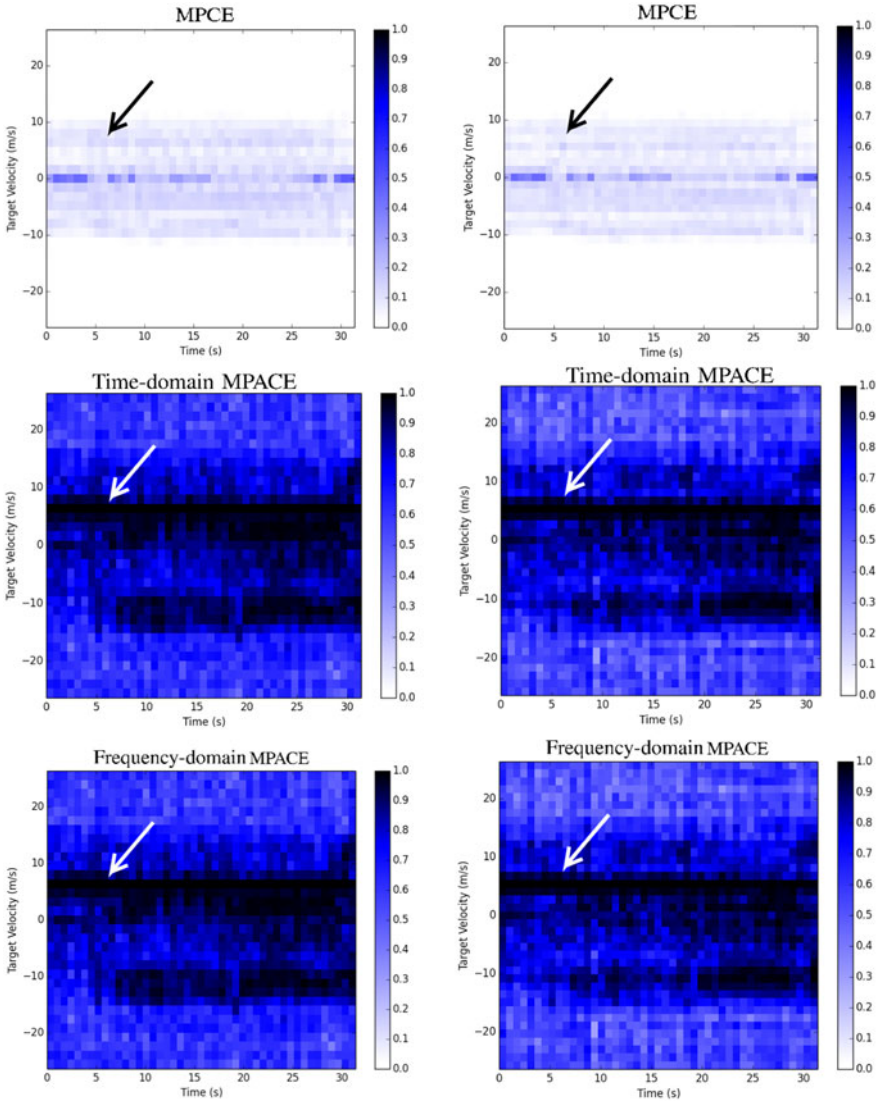

Fig. 3. MPCE and MPACE scores for synthetic point target scenario. The target is added to real WTC at 0 dB output signal-to-noise ratio (SNR) and moving at 6.0 m/sec; ideally this would appear as a dark horizontal band near the indicating arrow. In all figures, a resolution cell has dimensions λ_c/RT m/sec in velocity and MRT s in time. (Top row) MPCE detection score, from left to right, for $R = 21, 24$. The target is not visible within the wind turbine clutter, and very little if any improvement is observed from increasing the coherent processing interval. (Center row) The same scenario, using the time-domain MPACE score. (Bottom row) The same scenario, using the frequency-domain MPACE score. The target becomes more visible and the clutter is better mitigated as R increases from left to right. In all three examples, K is chosen to be two, so that the 669×669 clutter covariance matrix is approximated by a block-diagonal matrix with blocks of size 42 and 48, respectively.

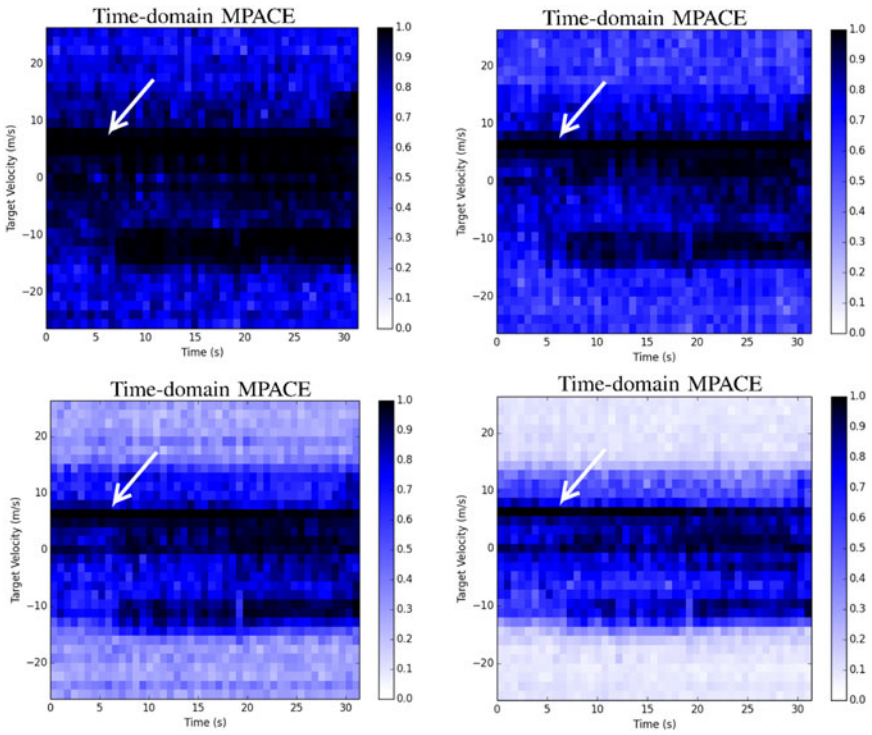

Fig. 4. Demonstration of improvement in clutter whitening due to improvement in the block-diagonal approximation to the clutter covariance. Again, a target has been added at 0 dB output SNR, moving at 6.0 m/s. The expected target velocity is indicated by the arrow. All four score histories were calculated with $R = 21$. (Top row) Time-domain MPACE scores for $K = 1, 2$. (Bottom row) Time-domain MPACE scores for $K = 3, 4$. As K increases, the wind turbine clutter is better whitened.

reasonably close to the turbine's nominal operating frequency of 29 r/min. For our experiments in this section, the first 42 s of the pulse history were divided into a training set (≈10 turbine periods) and a test set (≈10 turbine periods). In each experiment, an ideal point scatterer moving at a fixed velocity is synthetically added to the test data. The target strength is adjusted so that the output signal-to-noise ratio (SNR) of the R-pulse matched filter is approximately 0 dB. We always choose M so that MRT is approximately one third of a turbine rotation, which is roughly 0.6 s. We caution the reader that Fig. 2 is used for qualitative insight only. Nowhere in our theory do we use a short-term Fourier transform of the data to implement our detectors. Moreover, our only use of cyclostationarity is to argue that the correlation structure of the wind turbine clutter repeats itself every MR pulses.

The first experiment is to demonstrate the increase in coherent gain obtained by increasing the length of the coherent processing interval, R. We add a target moving at a range-rate of 6.0 m/s to the test data, and calculate coherence scores for a range of candidate target velocities and for each consecutive interval of length MRT. In each case, we compare the detectors in (35) and (42) against the MPCE score

$$1 - \prod_{m=0}^{M-1} \left(1 - \frac{|\psi_R^H(\theta)\mathbf{y}_m|^2}{||\psi_R(\theta)||^2||\mathbf{y}_m||^2}\right) = 1 - \prod_{m=0}^{M-1} \left(1 - \frac{\mathbf{y}_m^H \mathbf{P}_{\psi_R(\theta)}\mathbf{y}_m}{\mathbf{y}_m^H \mathbf{y}_m}\right). \quad (43)$$

This amounts to choosing $K = 1$ and $\mathbf{R} = \mathbf{I}$ in the time-domain ACE detector. The results of both MPACE and MPCE detectors for $R = 21$ and 24 are shown in Fig. 3.

The second experiment is to demonstrate the improvement in clutter whitening associated with increasing the block size K of the block-diagonal approximation to the clutter covariance. Ideally, one would use a sufficient amount of training data to ensure that the sample covariance $\mathbb{E}[\mathbf{w}_n \mathbf{w}_n^H]$ is a well conditioned, reliable estimate of the clutter covariance. However, due to changing weather conditions, it may be difficult or impossible to gather a sufficient quantity of training data. A larger K corresponds to a better approximation, assuming that at least KR samples of training data are available. The results of the MPCE and MPACE detectors for $R = 18$ and $K = 1, 2, 3$, and 4 are shown in Fig. 4.

C. Airplane Superimposed Over Turbine Clutter

In addition to the wind turbine data used in this section, we obtained an additional set of data recorded using the CSU-CHILL platform, which observed an unidentified aircraft maneuvering through its line of sight, with minimal stationary clutter. This data was recorded with the same system parameters (center frequency, pulse duration, etc.) as the WTC data, with the sole exception that the PRF was changed to 1 kHz. In particular, the maximum unambiguous velocity range is ±25 m/sec. To obtain a more realistic set of training data to test our detectors on, we resampled the WTC data to the same PRF as the airplane data and

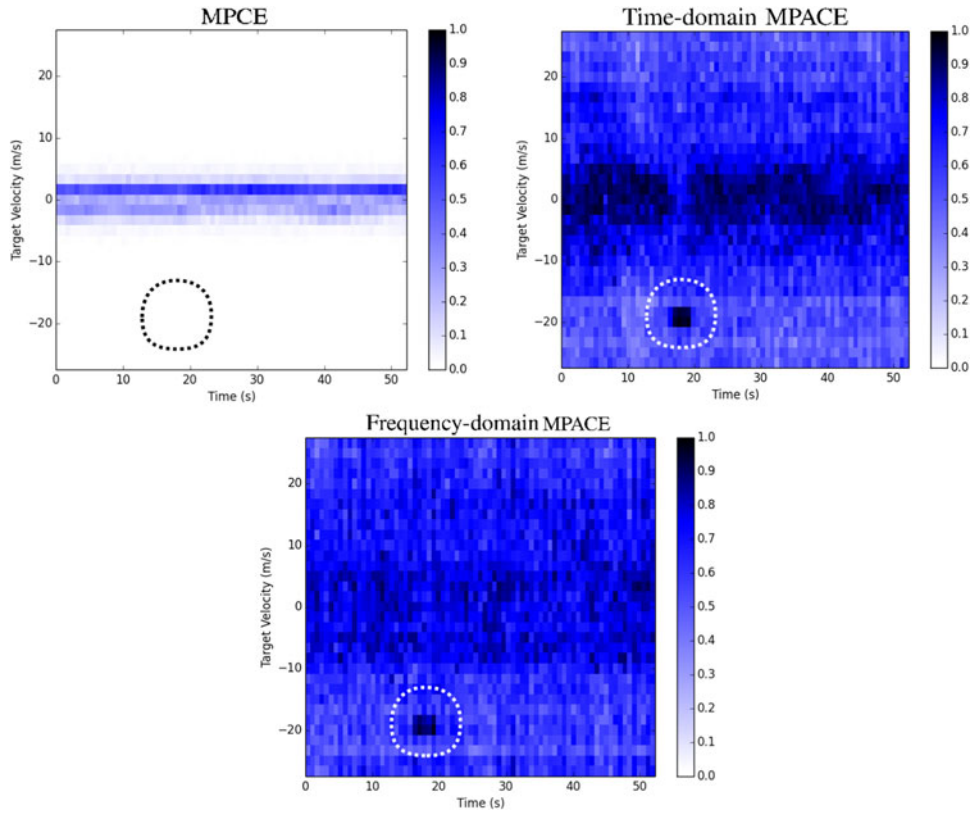

Fig. 5. Detection histories for the airplane scenario; target is approximately −24 dB relative to clutter. Expected target velocity (after aliasing) and time extent of the airplane is within the dotted circle. (Top Left) MPCE. (Top Right) Time-domain MPACE detector with $R = 21$ and $K = 3$. (Bottom) Frequency-domain MPACE detector with $R = 21$ and $K = 3$.

superimposed the two pulse histories to obtain the pulse history of a single, synthetic range bin containing both airplane and turbine. The airplane's input SNR is approximately −24 dB relative to the turbine. The target is present in the range bin in question for approximately two seconds, starting eighteen seconds into the dataset, moving at a nominal velocity of −70 m/s. As this is outside the maximum unambiguous velocity range, we observe instead an aliased copy of the airplane at an apparent velocity of −20 m/s.

We repeat the previous experiment, noting that the airplane is rendered nearly undetectable by the MPCE detector. The time-domain and frequency-domain MPACE detectors are able to separate the target from the clutter for many choices of pulse train length R and block-diagonal covariance approximation parameter K, but for brevity we present an example with $R = 21$ and $K = 3$ in Fig. 5.

VI. CONCLUSION

In this paper, we have derived a measurement model for target and clutter in a pulse-Doppler radar system. The model has three design parameters: R is the number of consecutive pulses over which baseband phase increases linearly in response to a constant velocity target; M is the number of such R-pulse trains over which a target remains in a given range bin; and K is the parameter that models the $MR \times MR$ wind clutter covariance as a block-diagonal matrix of N different $KR \times KR$ blocks.

This measurement model is then used to derive a GLR test. This test is a threshold test that uses a multipulse coherence statistic, MPACE, consisting of an incoherent geometric average of coherently computed ACE scores. Each ACE score is an adaptive coherence estimator between an KR-dimensional measurement and a K-dimensional subspace of $\mathbb{C}^{KR}$. The KR-dimensional measurement is the output of KR consecutive range-compressed samples.

Experimental results demonstrate that the coherence detector approximately whitens wind turbine clutter and detects 0 dB targets embedded in the dominant clutter band of the wind turbine.

VII. POST-SCRIPT

We refer the reader to [28] for an account of the provenance for first-order coherence detectors, including ACE and related detectors. This provenance includes the original work of Kelly, [31], Kelly and Forsythe, [32], Chen and Reed, [33], Robey *et al.*, [34], [35], and Conte *et al.*, [36], [37]. Conte *et al.* papers, based on asymptotics in a Bayesian model, slightly predate the rank-1 version of ACE, based on estimate and plug in a Fisherian model, presented in [27], [38], [39]. But ACE is essentially a story in uniformly most powerful invariant (UMPI) detection of multirank subspace signals. With the publication of [28]–[30] we now have a full understanding of ACE, its invariances, its optimalities, and its performances.

At the IEEE Radar Conference in Seattle, May 8–12, 2017, we were alerted to [40], where the MPCE statistic, for the rank-one case $K = 1$ was reported in 2015 by Abramovich and Besson. The statistic was found as an approximation of a GLRT. The likelihood of measurements was derived for a sequence of measurements that were *conditionally* complex Gaussian with covariance $\tau_n \mathbf{R}$, with the texture parameter τ distributed as a Gamma random variable. Then the joint distribution of the measurement and the texture was marginalized with respect to the Gamma distribution to obtain a likelihood that was then approximated by a monotone function of the MPCE statistic. So our MPACE, which accomodates multirank signals and uses secondary data to estimate the covariance $\mathbf{R}$, is an adaptive version of MPCE. Moreover, as we shall show in a paper currently under review [41], the result of [40] may be derived without appealing to a Gamma law for the unknown textures τ_n, instead treating them as unknown parameters in an unconditional Gaussian distribution for the measurements.

In summary, there is an MPCE, Bayesian [40], and Fisherian [41]. There is an MPACE. MPACE is adaptive from secondary data. MPCE is nonadaptive. So MPACE bears the same connection to MPCE that ACE bears to CFAR MSD [35].

ACKNOWLEDGMENT

The authors are grateful to V. Chandrasekar for providing the CHILL data, and to R. Beauchamp for help with its interpretation. They also thank D. Cochran for many helpful discussions. Consequently, the US Government is authorized to reproduce and distribute reprints for governmental purposes notwithstanding any copyright notation thereon. The views and conclusions contained herein are those of the authors and should not be interpreted as necessarily representing the official policies or endorsements, either expressed or implied, of the Air Force Research Laboratory or the US Government.

REFERENCES

[1] G. J. Poupart
Wind farms impact on radar aviation interests – Final report
QinetiQ Ltd, Waltham, MA, USA, Tech. Rep. W/14/00614/REP, Sep. 2003.

[2] J. Perry and A. Biss
Wind farm clutter mitigation in air surveillance radar
IEEE Aerosp. Electron. Syst. Mag., vol. 22, no. 7, pp. 35–40, Jul. 2007.

[3] G. Greving, W.-D. Biermann, and R. Mundt
Radar and wind turbines—RCS theory and results for objects on the ground and in finite distances
In *Proc. Microw., Radar Remote Sens. Symp.*, Aug. 2011, pp. 321–326.

[4] J. J. McDonald *et al.*,
Radar-cross-section reduction of wind turbines
Sandia, Albuquerque, NM, Tech. Rep., Mar. 2012.

[5] A. Naqvi, S.-T. Yang, and H. Ling
Investigation of Doppler features from wind turbine scattering
IEEE Antennas Wireless Propag. Lett., vol. 9, pp. 485–488, 2010.

[6] N. Whitelonis, S.-T. Yang, and H. Ling
Application of near-field to far-field transformation to Doppler features from wind turbine scattering
IEEE Trans. Antennas Propag., vol. 60, no. 3, pp. 1660–1665, Mar. 2012.

[7] A. Sterns, L. Manuel, K. Saranyasoontorn, and L. Nelson
Analysis of time series data on wind turbine loads
Nat. Sci. Found., Arlington, VA, USA, Tech. Rep., 2003.

[8] S. Manzato, B. Peeters, R. Osgood, and M. Luczak
Wind turbine model validation by full-scale vibration test
In *Proc. Eur. Wind Energy Conf.*, 2010, vol. 11, pp. 395–409.

[9] P. J. Schubel and R. J. Crossley
Wind turbine blade design
Energies, vol. 5, no. 9, pp. 3425–3449, 2012. [Online]. Available: http://www.mdpi.com/1996-1073/5/9/3425

[10] A. Shchuka and I. Sandhu
Air traffic control wind turbine interference mitigation at Raytheon, 2012. [Online]. Available: http://www.raytheon.com/newsroom/technology_today/2012_i2/airtraffic.html

[11] M. Jahangir
Target centric wide-area 3-D surveillance using a non-scanning multibeam receiver array
In *Proc. 2015 IEEE Radar Conf.*, May 2015, pp. 0652–0657.

[12] M. Jahangir and T. Quilter
The practicality and benefit of a 3-D wide-area persistent surveillance micro-doppler radar
In *Proc. 2015 16th Int. Radar Symp.*, Jun. 2015, pp. 272–277.

[13] A. D. Siggia and R. E. Passarelli
Gaussian model adaptive processing (GMAP) for improved ground clutter cancellation and moment calculation
In *Proc. 3rd Eur. Conf. Radar Meteorol. Hydrol.*, 2004, pp. 67–73.

[14] M. Butler and D. Johnson
Feasibility of mitigating the effects of wind farms on primary radar
RenewableUK, London, U.K., Tech. Rep. W1400623, 2003.

[15] C. Jackson and M. Butler
Options for mitigation of the effects of wind farms on radar sytems
In *Proc. Int. Conf. Radar Syst.*, Oct. 2007, pp. 1–6.

[16] R. Palmer, K. Le, and B. Isom
Wind turbine clutter mitigation using fully adaptive arrays
In *Proc. Eur. Radar Conf.*, Oct. 2008, pp. 356–359.

[17] K. T. Hood, S. Torres, and R. Palmer
Automatic detection of wind turbine clutter using Doppler spectral features
In *Proc. 34th Int. Conf. Radar Meteorol.*, 2009.

[18] K. Hood, S. Torres, and R. Palmer
Automatic detection of wind turbine clutter for weather radars
J. Atmos. Ocean. Technol., vol. 27, pp. 1868–1880, Nov. 2010.

[19] F. Kong, Y. Zhang, and R. Palmer
Wind turbine clutter mitigation for weather radar by adaptive spectrum processing
In *Proc. IEEE Radar Conf.*, May 2012, pp. 471–474.

[20] W. Melvin and J. Guerci
Knowledge-aided signal processing: A new paradigm for radar and other advanced sensors
IEEE Trans. Aerosp. Electron. Syst., vol. 42, no. 3, pp. 983–996, Jul. 2006.

[21] F. Nai, R. D. Palmer, and S. M. Torres
Range-Doppler domain signal processing to mitigate wind turbine clutter
In *Proc. IEEE Radar Conf.*, May 2011, pp. 841–845.

[22] B. Gallardo-Hernando, F. Pérez-Martínez, and F. Aguado-Encabo
Mitigation of wind turbine clutter in C-band weather radars for different rainfall rates
In *Proc. Int. Radar Conf.*, Oct. 2009, pp. 1–6.

[23] B. Isom *et al.*,
Characterization and mitigation of wind turbine clutter on the WSR-88D network
In *Proc. 33rd Conf. Radar Meteorol.*, Aug. 2007.

[24] B. Isom *et al.*,
Detailed observations of wind turbine clutter with scanning weather radars
J. Atmos. Ocean. Technol., vol. 26, no. 5, pp. 894–910, 2009. [Online]. Available: http://dx.doi.org/10.1175/2008JTECHA1136.1

[25] A. Naqvi and H. Ling
Signal filtering technique to remove Doppler clutter caused by wind turbines
Microw. Opt. Technol. Lett., vol. 54, no. 6, pp. 1455–1460, 2012. [Online]. Available: http://dx.doi.org/10.1002/mop.26819

[26] F. Uysal, U. Pillai, I. Selesnick, and B. Himed
Signal decomposition for wind turbine clutter mitigation
In *Proc. IEEE Radar Conf.*, May 2014, pp. 60–63.

[27] L. L. Scharf and L. T. McWhorter
Adaptive matched subspace detectors and adaptive coherence estimators
In *Proc. 30th Asilomar Conf. Signals, Syst. Comput.*, 1996, pp. 1114–1117.

[28] S. Kraut, L. L. Scharf, and L. T. McWhorter
Adaptive subspace detectors
IEEE Trans. Signal Process., vol. 49, no. 1, pp. 1–16, Jan. 2001.

[29] S. Kraut and L. L. Scharf
The CFAR adaptive subspace detector is a scale-invariant GLRT
IEEE Trans. Signal Process., vol. 47, no. 9, pp. 2538–2541, Sep. 1999.

[30] S. Kraut, L. L. Scharf, and R. W. Butler
The adaptive coherence estimator: A uniformly most-powerful-invariant adaptive detection statistic
IEEE Trans. Signal Process., vol. 53, no. 2, pp. 427–438, Feb. 2005.

[31] E. J. Kelly
An adaptive detection algorithm
IEEE Trans. Aerosp. Electron. Syst., vol. AES-22, no. 2, pp. 115–127, Mar. 1986.

[32] E. J. Kelly and K. M. Forsythe
Adaptive detection and parameter estimation for multidimensional signal models
Lincoln Lab., Massachusetts Inst. Technol., Lexington, MA, USA, Tech. Rep. 848, 1989.

[33] W.-S. Chen and I. S. Reed
A new CFAR detection test for radar
Digit. Signal Process., vol. 1, no. 4, pp. 198–214, 1991.

[34] F. C. Robey, D. R. Fuhrmann, E. J. Kelly, and R. Nitzberg
A CFAR adaptive matched filter detector
IEEE Trans. Aerosp. Electron. Syst., vol. 28, no. 1, pp. 208–216, Jan. 1992.

[35] L. L. Scharf and B. Friedlander
Matched subspace detectors
IEEE Trans. Signal Process., vol. 42, no. 8, pp. 2146–2157, Aug. 1994.

[36] E. Conte, M. Lops, and G. Ricci
Asymptotically optimum radar detection in compound-Gaussian clutter
IEEE Trans. Aerosp. Electron. Syst., vol. 31, no. 2, pp. 617–625, Apr. 1995.

[37] E. Conte, M. Lops, and G. Ricci
Adaptive matched filter detection in spherically invariant noise
IEEE Signal Process. Lett., vol. 3, no. 8, pp. 248–250, Aug. 1996.

[38] L. L. Scharf
Adaptive matched subspace detectors and adaptive coherence
Univ. Colorado Boulder, Boulder, CO, USA, Tech. Rep., Jun. 1996.

[39] L. T. McWhorter, L. L. Scharf, and L. J. Griffiths
Adaptive coherence estimation for radar signal processing
In *Proc. Conf. Record 30th Asilomar Conf. Signals, Syst. Comput.*, Nov. 1996, vol. 1, pp. 536–540.

[40] Y. I. Abramovich and O. Besson
Fluctuating target detection in fluctuating k-distributed clutter
IEEE Signal Process. Lett., vol. 22, no. 10, pp. 1791–1795, Oct. 2015.

[41] P. Pakrooh and L. L. Scharf
Multipulse subspace detectors
In *Proc. Asilomar Conf. Signals, Syst. Comput*.

Pooria Pakrooh (S'13–M'17) received the B.Sc. degree in electrical engineering from Iran University of Science and Technology, Tehran, Iran, in 2008, the M.Sc. degree in electrical engineering from Sharif University of Technology, Tehran, Iran, in 2011, and the Ph.D. degree in electrical engineering from Colorado State University, Fort Collins, CO, USA, in 2015.

He is currently a Postdoctoral Research Associate in the Department of Mathematics, Colorado State University. His current research interests include compressed sensing and statistical signal processing, and their applications in sensor and array signal processing.

Andrew Homan (M'16) received the Ph.D. degree in mathematics from Purdue University, West Lafayette, IN, USA in 2015.

His research interests include signal processing and microlocal analysis. He is currently a Research Engineer at Matrix Research, Dayton, OH, USA.

Louis L. Scharf (S'67–M'69–SM'77–F'86–LF'07) received the Ph.D. degree from the University of Washington, Seattle, WA, USA.

From 1971 to 1982, he served as a Professor of electrical engineering and statistics at Colorado State University, Fort Collins, CO, USA. From 1982 to 1985, he was a Professor and Chair of electrical and computer engineering with the University of Rhode Island, Kingston, RI, USA. From 1985 to 2001, he was a Professor of electrical and computer engineering with the University of Colorado, Boulder, CO, USA. In January 2001 he rejoined Colorado State University as a Professor of electrical and computer engineering, and statistics. He is currently a Research Professor of mathematics and emeritus professor of electrical and computer engineering, with a joint appointment in statistics at Colorado State University. He has held visiting positions here and abroad, including Duke University, University of Wisconsin, Ecole Superieure d'Electricite, Ecole Superieure des Telecommunications, EURECOM, University of La Plata, University of Tromso, University of Newcastle, and University of Paderborn. His research interests include statistical signal processing, as it applies to adaptive radar and sonar, communication, and electric power. He has made original contributions to matched and adaptive subspace detection for radar, sonar, and hyperspectral imaging; invariance theories for detection and estimation in subspaces; reduced-rank signal processing for compression and reduced-rank filtering; multichannel coherence for space-time signal processing; and modal analysis in power systems. He has authored three books: L.L. Scharf, "Statistical Signal Processing: Detection, Estimation, and Time Series Analysis (Addison-Wesley, 1991); L.L. Scharf, A First Course in Electrical and Computer Engineering (Addison-Wesley, 1998); and P.J. Schreier and L.L. Scharf, Statistical Signal Processing of Complex-Valued Data: The Theory of Improper and Noncircular Signals" (Cambridge University Press, 2010).

Prof. Scharf was Technical Program Chair for the 1980 IEEE International Conference on Acoustics, Speech, and Signal Processing (ICASSP), Tutorials Chair for ICASSP 2001; and Technical Program Chair for the Asilomar Conference on Signals, Systems, and Computers, 2002. He is past Chair of the Fellow Committee for the IEEE Signal Processing Society. He has received several awards for his professional service and his contributions to statistical signal processing, including the IEEE Distinguished Lectureship, the IEEE Third Millennium Medal, the Technical Achievement and Society Awards from the IEEE Signal Processing Society, the Donald W. Tufts Award for Underwater Acoustic Signal Processing, a 2016 Diamond Award from the University of Washington (Seattle), and the 2016 IEEE Jack S. Kilby Signal Processing Medal, endowed by Texas Instruments.

Margaret Cheney is the Albert C. Yates Endowment Professor of mathematics at Colorado State University (CSU), Fort Collins, CO, USA, where she also holds an appointment in the Department of Electrical and Computer Engineering. Before moving to CSU in 2012, she was a Professor at Rensselaer Polytechnic Institute for many years. In 2000, she was the Lise Meitner Visiting Professor at Lund Institute of Technology. She has served on the editorial boards of five journals. Most of her work has been on the inverse problems that arise in acoustics and electromagnetics; since 2001, she has been working on radar imaging.

Prof. Cheney was awarded an Honorary Doctor of Science by Oberlin College in 2011. She is a Fellow of the Institute of Physics and a Fellow of SIAM.

Matthew Ferrara (M'09) received the B.S. degree in mathematics at North Dakota State University, Fargo, ND, USA, in 2003, the M.S. and Ph.D. degrees in mathematics from Rensselaer Polytechnic Institute, Troy, NY, USA, in 2004 and 2006, respectively.

He is currently a Program Lead in Matrix Research, Dayton, OH, USA. From 2006 to 2010, he was a Research Mathematician for the Air Force Research Laboratory's Sensors Directorate in Dayton, OH, USA. His work is primarily focused on electromagnetic sensor signal processing.